Catch-Disperse-Release Readout for Superconducting Qubits

Eyob A. Sete[1], Andrei Galiautdinov[1,2], Eric Mlinar[1], John M. Martinis[3], and Alexander N. Korotkov[1]
[1]*Department of Electrical Engineering, University of California, Riverside, California 92521, USA*
[2]*Department of Physics and Astronomy, University of Georgia, Athens, Georgia 30602, USA*
[3]*Department of Physics, University of California, Santa Barbara, California 93106, USA*
(Dated: March 1, 2013)

We analyze single-shot readout for superconducting qubits via controlled catch, dispersion, and release of a microwave field. A tunable coupler is used to decouple the microwave resonator from the transmission line during the dispersive qubit-resonator interaction, thus circumventing damping from the Purcell effect. We show that if the qubit frequency tuning is sufficiently adiabatic, a fast high-fidelity qubit readout is possible even in the strongly nonlinear dispersive regime. Interestingly, the Jaynes-Cummings nonlinearity leads to the quadrature squeezing of the resonator field below the standard quantum limit, resulting in a significant decrease of the measurement error.

PACS numbers: 03.67.Lx, 03.65.Yz, 42.50.Pq, 85.25.Cp

Introduction.–Fast high-fidelity qubit readout plays an important role in quantum information processing. For superconducting qubits various nonlinear processes have been used to realize a single-shot readout [1–6]. Linear dispersive readout in the circuit quantum electrodynamics (cQED) setup [7, 8] became sufficiently sensitive for the single-shot qubit measurement only recently [9, 10], with development of near-quantum-limited superconducting parametric amplifiers [9–11]. In particular, readout fidelity of 94% for flux qubits [9] and 97% for transmon qubits [10] has been realized (see also [12]). With increasing coherence time of superconducting qubits into 10-100 μs range [13, 14], fast high-fidelity readout becomes practically important, for example, for reaching the threshold of quantum error correction codes [15], for which the desired readout time is less than 100 ns, with fidelity above 99%.

A significant source of error in the currently available cQED readout schemes is the Purcell effect [16] — the cavity-induced relaxation of the qubit due to the always-on coupling between the resonator and the outgoing transmission line. The Purcell effect can be reduced by increasing the qubit-resonator detuning; however, this reduces the dispersive interaction and increases measurement time. Several proposals to overcome the Purcell effect have been put forward, including the use of the Purcell filter [17] and the use of a Purcell-protected qubit [18]. Here we propose and analyze a cQED scheme which avoids the Purcell effect altogether by decoupling the resonator from the transmission line during the dispersive qubit-resonator interaction.

Main idea and results.–Similar to the standard cQED measurement [7–10], in our method (Fig. 1) the qubit state affects the dispersive shift of the resonator frequency, that in turn changes the phase of the microwave field in the resonator, which is then measured via homodyne detection. However, instead of measuring continuously, we perform a sequence of three operations: "catch", "disperse", and "release" of the microwave field. During the first two stages a tunable coupler [19, 20] decouples the outgoing transmission line from the resonator. This automatically eliminates the problems associated with the Purcell effect, as coupling to the incoming microwave line can be made very small [20].

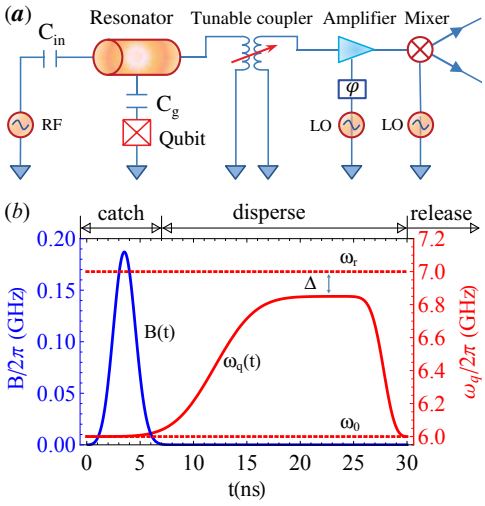

FIG. 1: (color online). a) Schematic of the measurement setup. The radio frequency (RF) source produces a microwave pulse, which populates the resonator via a small capacitor $C_{\rm in}$. The resonator photons then interacts with a capacitively ($C_{\rm g}$) coupled qubit. The interaction with the outgoing transmission line is controlled by a tunable coupler, which releases photons at the end of the procedure. The released field is then amplified and mixed with the local oscillator (LO) signal to be measured via homodyne detection. b) The RF pulse $B(t)$ (blue curve) and varying qubit frequency $\omega_{\rm q}(t)$ (red curve), with approximate indication of the "catch", "disperse", and "release" stages. Dashed lines show the resonator frequency $\omega_{\rm r}$ and initial/final qubit frequency ω_0; $\Delta = \omega_{\rm r} - \omega_{\rm q}$ is the detuning at the "disperse" stage.

During the "catch" stage, the initially empty resonator is driven by a microwave pulse and populated with $\sim$10 photons. At this stage the qubit is far detuned from the resonator [Fig. 1(b)], which makes the dispersive coupling negligible and allows the creation of an almost-perfect coherent state in the resonator. At the next "disperse" stage of the measurement, the qubit frequency is adiabatically tuned closer to the resonator frequency to produce a strong qubit-resonator in-

Report Documentation Page

Form Approved
OMB No. 0704-0188

1. REPORT DATE	2. REPORT TYPE	3. DATES COVERED
01 MAR 2013		**00-00-2013 to 00-00-2013**

4. TITLE AND SUBTITLE	5a. CONTRACT NUMBER
Catch-Disperse-Release Readout for Superconducting Qubits	5b. GRANT NUMBER
	5c. PROGRAM ELEMENT NUMBER
6. AUTHOR(S)	5d. PROJECT NUMBER
	5e. TASK NUMBER
	5f. WORK UNIT NUMBER
7. PERFORMING ORGANIZATION NAME(S) AND ADDRESS(ES) **University of California, Santa Barbara,Department of Physics,Santa Barbara,CA,93106**	8. PERFORMING ORGANIZATION REPORT NUMBER
9. SPONSORING/MONITORING AGENCY NAME(S) AND ADDRESS(ES)	10. SPONSOR/MONITOR'S ACRONYM(S)
	11. SPONSOR/MONITOR'S REPORT NUMBER(S)

12. DISTRIBUTION/AVAILABILITY STATEMENT
Approved for public release; distribution unlimited

13. SUPPLEMENTARY NOTES

14. ABSTRACT

15. SUBJECT TERMS

16. SECURITY CLASSIFICATION OF:			17. LIMITATION OF ABSTRACT	18. NUMBER OF PAGES	19a. NAME OF RESPONSIBLE PERSON
a. REPORT **unclassified**	b. ABSTRACT **unclassified**	c. THIS PAGE **unclassified**	**Same as Report (SAR)**	**5**	

teraction (it may even be pushed into the nonlinear regime). During this interaction, the resonator field amplitudes ($\lambda_{\rm eff}$) associated with the initial qubit states $|0\rangle$ and $|1\rangle$ rapidly accumulate additional phases and separate in the complex phase plane [see Fig. 2(a)]. Finally, at the last "release" stage of the measurement, after the qubit frequency is again detuned from the resonator, the resonator photons are released into the outgoing transmission line. The signal is subsequently amplified (by a phase-sensitive parametric amplifier) and sent to the mixer where the homodyne detection is performed.

With realistic parameters for superconducting qubit technology, we numerically show that the measurement of 30–40 ns duration can be realized with an error below 10^{-3}, neglecting the intrinsic qubit decoherence. The latter assumption requires the qubit coherence time to be over 40 μs, which is already possible experimentally [14]. It is interesting that because of the interaction nonlinearity [21, 22], increasing the microwave field beyond $\sim$10 photons only slightly reduces the measurement time. The nonlinearity also gives rise to about $\sim$50% squeezing of the microwave field, which provides an order-of-magnitude reduction of the measurement error.

The model.–We consider a superconducting phase or transmon qubit capacitively coupled to a microwave resonator [Fig. 1(a)]. For simplicity we start with considering a two-level qubit (the third level will be included later) and describe the system by the Jaynes-Cummings (JC) Hamiltonian [7] with a microwave drive (we use $\hbar = 1$)

$$H = \omega_{\rm q}(t)\sigma_+\sigma_- + \omega_{\rm r}a^\dagger a + g(a\sigma_+ + \sigma_- a^\dagger) + B(t)a^\dagger e^{-i\omega t} + B^*(t)ae^{i\omega t}, \quad (1)$$

where $\omega_{\rm q}(t)$ and $\omega_{\rm r}$ are, respectively, the qubit and the resonator frequencies, $\sigma_\pm$ are the rasing and lowering operators for the qubit, a ($a^\dagger$) is the annihilation (creation) operator for the resonator photons, g (assumed real) is the qubit-resonator coupling, $B(t)$ and ω are the effective amplitude and the frequency of the microwave drive, respectively. In this work we assume $\omega = \omega_{\rm r}$.

For the microwave drive $B(t)$ and the qubit frequency $\omega_q(t)$ [Fig. 1(b)] we use Gaussian-smoothed step-functions: $B(t) = 0.5B_0\{{\rm Erf}[(t-t_{\rm B})/\sqrt{2}\sigma_{\rm B}] - {\rm Erf}[(t-t_{\rm B}-\tau_{\rm B})/\sqrt{2}\sigma_{\rm B}]\}$ and $\omega_{\rm q}(t) = \omega_0 + 0.5(\Delta_0-\Delta)\{{\rm Erf}[(t-t_{\rm q})/\sqrt{2}\sigma_{\rm q}] - {\rm Erf}[(t-t_{\rm qe})/\sqrt{2}\sigma_{\rm qe}]\}$, where $t_{\rm B}$, $t_{\rm B}+\tau_{\rm B}$, $t_{\rm q}$, and $t_{\rm qe}$ are the centers of the front/end ramps, and $\sigma_{\rm B}$, $\sigma_{\rm q}$, and $\sigma_{\rm qe}$ are the corresponding standard deviations. In numerical simulations we use $\sigma_{\rm B} = \sigma_{\rm qe} = 1$ ns (typical experimental value for a short ramp) while we use longer $\sigma_{\rm q}$ to make the qubit front ramp more adiabatic. Other fixed parameters are: $g/2\pi = 30$ MHz, $\tau_{\rm B} = 1$ ns, $t_{\rm B} = 3$ ns, $\omega_{\rm r}/2\pi = 7$ GHz, and $\omega_0/2\pi = 6$ GHz, so that initial/final detuning $\Delta_0 = \omega_{\rm r} - \omega_0$ is 1 GHz, while the disperse-stage detuning Δ is varied. The measurement starts at $t = 0$ and ends at $t_{\rm f} = t_{\rm qe} + 2\sigma_{\rm qe}$ when the field is quickly released [23].

Simplified analysis.–Let us first consider a simple dispersive scenario at large qubit-resonator detuning, $|\Delta| \gg g\sqrt{\overline{n}+1}$, where $\overline{n}$ is the average number of photons in the resonator. In this case, the system is described by the usual dispersive Hamiltonian [7] $H_d = (\omega_0 + g^2/\Delta)\sigma_z/2 + (\omega_r + \sigma_z g^2/\Delta)a^\dagger a$, where σ_z is the Pauli matrix. After the short "catch" stage the system is in a product state $(\alpha|0\rangle + \beta|1\rangle)|\lambda_{\rm in}\rangle$, where α and β are the initial qubit state amplitudes and $\lambda_{\rm in}$ is the amplitude of the coherent resonator field, $\lambda_{\rm in} = -i\int B(t)\,dt$ (so $\overline{n} = |\lambda_{\rm in}|^2$). Then during the "disperse" stage the qubit-resonator state becomes entangled, $\alpha|0\rangle|\lambda_0(t)\rangle + \beta|1\rangle|\lambda_1(t)\rangle$, with $\lambda_0 = \lambda_{\rm in}e^{-i\phi}$, $\lambda_1 = \lambda_{\rm in}e^{i\phi}$, and $\phi(t) = \int_0^t [g^2/\Delta(t')]dt'$.

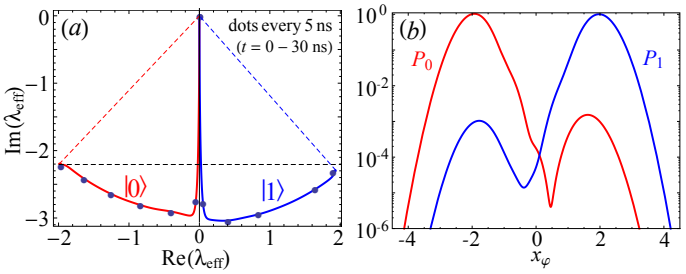

FIG. 2: (color online). (a) Evolution in time of the effective field amplitude $\lambda_{\rm eff}$ on the complex phase plane for initial qubit states $|0\rangle$ and $|1\rangle$, computed numerically. The horizontal line emphasizes slight asymmetry. The dots indicate time moments $t = 0$, 5, 10, 15, 20, 25, and 30 ns. (b) Corresponding probability distributions $P_0(x_\varphi)$ and $P_1(x_\varphi)$ for measurement (at $t = t_{\rm f}$) of the optimum quadrature x_φ. Side bumps of P_0 and P_1 are due to non-adiabaticity. We used $g/2\pi = 30$ MHz, $\Delta/2\pi = 50$ MHz, $|\lambda_{\rm in}|^2 = 9$ ($B_0/2\pi = 497.4$ MHz, $\tau_{\rm B} = 1$ ns), $\sigma_{\rm q} = 3$ ns, $t_{\rm q} = 3.25$ ns, $t_{\rm qe} = 30$ ns, $t_{\rm B} = 3$ ns, and $t_{\rm f} = 32$ ns.

The distinguishablity of the two resonator states depends on their separation $|\delta\lambda| \equiv |\lambda_1 - \lambda_0| = 2|\lambda_{\rm in}|\sin|\phi|$ (see numerical results in Fig. 2). The released coherent states are measured via the homodyne detection using the optimal quadrature connecting λ_0 and λ_1, i.e. corresponding to the angle $\varphi = \arg(\lambda_1 - \lambda_0)$. We rescale the measurement results to the dimensionless field quadrature $\hat{x}_\varphi = (ae^{-i\varphi} + a^\dagger e^{i\varphi})/2$, which corresponds to the φ-angle axis in the phase space of Fig. 2(a). In resolving the two coherent states, we are essentially distinguishing two Gaussian probability distributions, $P_0(x_\varphi)$ and $P_1(x_\varphi)$, centered at $\pm|\delta\lambda|\sigma_{\rm coh}$ with $\sigma_{\rm coh} = 1/2$ being the coherent-state width (standard deviation) for both distributions. Then the measurement error has a simple form

$$E = \frac{1}{2}\int_{-\infty}^{\infty} \min(P_0, P_1)\,dx_\varphi = \frac{1 - {\rm Erf}(|\delta\lambda|\sqrt{\eta/2})}{2}, \quad (2)$$

where $\eta = \eta_{\rm col}\eta_{\rm amp}$ is the detection efficiency [24], which includes the collection efficiency $\eta_{\rm col}$ and quantum efficiency of the amplifier $\eta_{\rm amp}$. Unless mentioned otherwise, we assume $\eta = 1$, which corresponds to a quantum-limited phase-sensitive amplifier (for a phase-preserving amplifier $\eta \le 1/2$).

Full analysis.–In general the JC qubit-resonator interaction (1) is non-linear for $|\lambda_{\rm in}|^2 \gtrsim \Delta^2/4g^2$ [7] and the resonator states are not coherent. The measurement error E is still given by the first part of Eq. (2), while the probability distributions $P_{0,1}(x_\varphi)$ of the measurement result for the

qubit starting in either state $|0\rangle$ or $|1\rangle$ can be calculated in the following way. Assuming an instantaneous release of the field, we are essentially measuring the operator $\hat{x}_\varphi$. Therefore the probability $P(x_\varphi)$ for the ideal detection ($\eta = 1$) can be calculated by converting the Fock-space density matrix ρ_{nm} describing the resonator field, into the x_φ-basis, thus obtaining $P(x_\varphi) = \sum_{nm} \psi_n(x_\varphi)\rho_{nm}(t)\psi_m^*(x_\varphi)e^{-i(n-m)\varphi}$, where $\psi_n(x)$ is the standard nth-level wave function of a harmonic oscillator. For a non-instantaneous release of the microwave field the calculation of $P(x_\varphi)$ is non-trivial; however, since the qubit is already essentially decoupled from the resonator, the above result for $P(x_\varphi)$ remains the same [25] for optimal time-weighting of the signal. In the case of a non-ideal detection ($\eta < 1$) we should take a convolution of the ideal $P(x_\varphi)$ with the Gaussian of width $\sqrt{\eta^{-1} - 1}\,\sigma_{\rm coh}$. Calculation of the optimum phase angle φ minimizing the error is non-trivial in the general case. For simplicity we still use the natural choice $\varphi = \arg(\lambda_{\rm eff,1} - \lambda_{\rm eff,0})$, where the effective amplitude of the resonator field [26] is defined by $\lambda_{\rm eff} = \sum_n \sqrt{n}\rho_{n,n-1}$. The field density matrix ρ_{nm} is calculated numerically using the Hamiltonian (1) and then tracing over the qubit.

Extensive numerical simulations allowed us to identify two main contributions to the measurement error E in our scheme. The first contribution is due to the insufficient separation of the final resonator states $|\lambda_{\rm eff,1}\rangle$ and $|\lambda_{\rm eff,0}\rangle$, as described above. However, there are two important differences from the simplified analysis: the JC nonlinearity may dramatically change $|\delta\lambda|$ and it also produces a self-developing squeezing of the resonator states in the quadrature x_φ, significantly decreasing the error compared with Eq. (2) (both effects are discussed in more detail later). The second contribution to the measurement error is due to the nonadiabaticity of the front ramp of the qubit pulse $\omega_q(t)$, which leads to the population of "wrong" levels in the eigenbasis. This gives rise to the side peaks ("bumps") in the probability distributions $P_{0,1}(x_\varphi)$, as can be seen in Fig. 2(b) (notice their similarity to the experimental results [9, 10], though the mechanism is different). During the dispersion stage these bumps move in the "wrong" direction, halting the exponential decrease in the error, and thus causing the error to saturate. The nonadiabaticity at the rear ramp of $\omega_q(t)$ is not important because the moving bumps do not have enough time to develop. Therefore the rear ramp can be steep, while the front ramp should be sufficiently smooth [Fig. 1(a)] to minimize the error.

Now let us discuss the effect of nonlinearity (when $|\lambda_{\rm in}|^2 > \Delta^2/4g^2$) on the evolution of $\lambda_{\rm eff,0}$ and $\lambda_{\rm eff,1}$ during the disperse stage. Since the RF drive is turned off, the interaction described by the Hamiltonian (1) occurs only between the pairs of states $|0, n\rangle$ and $|1, n-1\rangle$ of the JC ladder. Therefore, if the front ramp of the qubit pulse is adiabatic, the pairs of the JC *eigenstates* evolve only by accumulating their respective phases while maintaining their populations. Then for the qubit initial state $|0\rangle$, the qubit-resonator wavefunction evolves approximately as $|\psi_0(t)\rangle \simeq e^{-|\lambda_{\rm in}|^2/2}\sum_n(\lambda_{\rm in}^n/\sqrt{n!})e^{-i\phi_{0,n}(t)}|\overline{0,n}\rangle$, where the overbar denotes the (dressed) eigenstate and $\phi_{0,n}(t) = \int_{t_{\rm D}}^t dt'[\sqrt{\Delta(t')^2 + 4g^2 n} - \Delta(t')]/2$ is the accumulated phase, with $t_{\rm D} = t_{\rm B} + \tau_{\rm B}/2$ being the center of the $B(t)$-pulse, which is crudely the start of the dispersion. Similarly, if the qubit starts in state $|1\rangle$ (following the ideology of Ref. [27], we then use $|\overline{10}\rangle$ as the initial state), the state evolves as $|\psi_1(t)\rangle \simeq e^{-|\lambda_{\rm in}|^2/2}\sum_n(\lambda_{\rm in}^n/\sqrt{n!})e^{i\phi_{1,n}(t)}|\overline{1,n}\rangle$, where $\phi_{1,n}(t) = \int_{t_{\rm D}}^t dt'[\sqrt{\Delta(t')^2 + 4g^2(n+1)} - \Delta(t')]/2$. Using the above definition of $\lambda_{\rm eff}$ and assuming $|\lambda_{\rm in}|^2 \gg 1$ we derive an approximate formula

$$\lambda_{\rm eff,0} = \lambda_{\rm in}\exp\left[-i\int_{t_{\rm D}}^t \frac{g^2}{\sqrt{\Delta(t')^2 + 4g^2|\lambda_{\rm in}|^2}}\,dt'\right]. \quad (3)$$

The corresponding expression for $\lambda_{\rm eff,1}$ can be obtained by replacing $-i$ with i and $|\lambda_{\rm in}|^2$ with $|\lambda_{\rm in}|^2 + 1$. These formulas agree well with our numerical results. In particular, they explain why $\lambda_{\rm eff,0}$ rotates slightly faster than $\lambda_{\rm eff,1}$, as seen in Fig. 2(a).

Equation (3) shows that a decrease in detuning leads to an increase in the rotation speed of $\lambda_{\rm eff}$. However, in the strongly nonlinear regime $|\lambda_{\rm in}|^2 \gg \Delta^2/4g^2$, the angular speed saturates at $d(\arg(\lambda_{\rm eff,0/1}))/dt = \mp g/2|\lambda_{\rm in}|$. Thus, the rate at which the $\lambda_{\rm eff,1}$ and $\lambda_{\rm eff,0}$ separate is limited by

$$d|\delta\lambda|/dt \le |g|, \quad (4)$$

which does not depend on $|\lambda_{\rm in}|$. This means that the measurement time should not improve much with increasing the mean number of photons $|\lambda_{\rm in}|^2$ in the resonator, as long as it is sufficient for distinguishing the states with a desired fidelity (crudely, $|\lambda_{\rm in}|^2 \gtrsim 7/\eta$ for $E \lesssim 10^{-4}$).

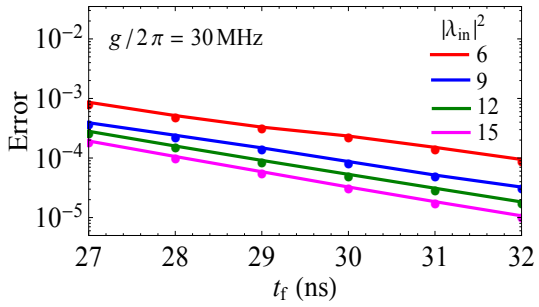

FIG. 3: (color online). Optimized measurement error E vs measurement time $t_{\rm f}$ (optimization is performed over Δ, $\sigma_{\rm q}$, and $t_{\rm q}$). The microwave pulses correspond to mean photon number $|\lambda_{\rm in}|^2 = 6, 9, 12$, and 15. The lines are guides for the eye.

Results of numerical optimization.–Figure 3 shows the results of a three-parameter optimization of the measurement error E for several values of the average number of photons in the resonator, $|\lambda_{\rm in}|^2$ (assuming $\eta = 1$). The optimization parameters are the qubit-resonator detuning Δ, the width σ_q, and the center t_q of the qubit front ramp. We see that for 9 photons in the resonator the error of 10^{-4} can be achieved with 30 ns measurement duration, excluding time to release

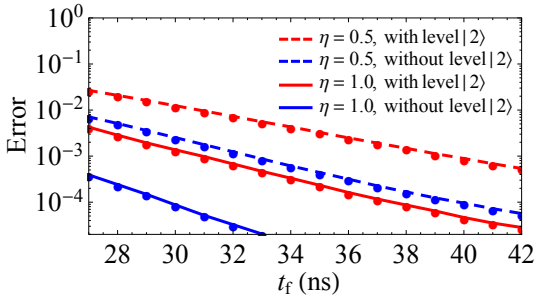

FIG. 4: (color online). Optimized error vs measurement time t_f for $|\lambda_{in}|^2 = 9$ and quantum efficiencies $\eta = 1$ or $\eta = 1/2$ (e.g. for a phase-preserving amplifier), taking into account the qubit level $|2\rangle$ (with anharmonicity $\mathcal{A}/2\pi = 200$ MHz) or assuming a two-level qubit.

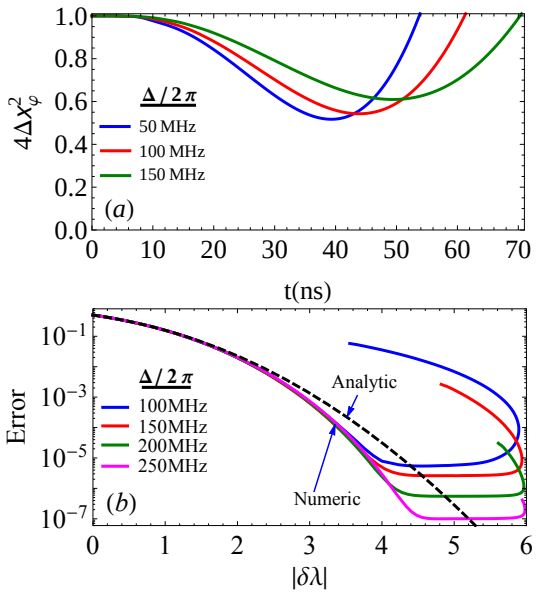

FIG. 5: (color online). (a) Time-evolution of the quadrature squeezing (the qubit is initially in state $|0\rangle$). (b) Measurement error vs $|\delta\lambda|$ obtained numerically (solid lines) and using Eq. (2) (dashed line); the evolution stops at 98 ns. Here $g/2\pi = 30$ MHz, $|\lambda_{in}|^2 = 9$, $\sigma_q = 4$ns, and $t_q = 3.25$ ns.

and measure the field. The optimum parameters in this case are: $\Delta/2\pi = 60$ MHz, $\sigma_q = 4.20$ ns, and $t_q = 3.25$ ns [this is a strongly nonlinear regime: $|\lambda_{in}|^2/(\Delta^2/4g^2) = 9$]. As expected from the above discussion, increasing the mean photon number to 12 and 15 shortens the measurement time only slightly (by 1 ns and 2 ns, keeping the same error). The dotted blue curve in Fig. 4 shows the optimized error for $|\lambda_{in}|^2 = 9$ and imperfect quantum efficiency $\eta = 1/2$. As we see, the measurement time for the error level of 10^{-4} increases to 40 ns, while the error of 10^{-3} is achieved at $t_f = 32$ ns.

So far, we considered the two-level model for the qubit. However, real superconducting qubits are only slightly anharmonic oscillators, so the effect of the next excited level $|2\rangle$ is often important. It is straightforward to include the level $|2\rangle$ into the Hamiltonian (1) by replacing its first term with $\omega_q|1\rangle\langle 1| + (2\omega_q - \mathcal{A})|2\rangle\langle 2|$, where $\mathcal{A}$ is the anharmonicity. The dispersion can then be understood as due to repulsion of three eigenstates: $|0,n\rangle$, $|1,n-1\rangle$, and $|2,n-2\rangle$. As the result, $\lambda_{eff,0}$ rotates on the phase plane faster than in the two-level approximation, while $\lambda_{eff,1}$ rotates slower (sometimes even in the opposite direction). The Supplemental Material [28] illustrates evolution of the resonator Wigner function corresponding to initial qubit states $|0\rangle$ and $|1\rangle$. The detailed description of the effect of level $|2\rangle$ is beyond the scope of this paper. Here we only show the optimized error for $\mathcal{A}/2\pi = 200$ MHz (a typical value for transmon and phase qubits), $|\lambda_{in}|^2 = 9$ and $\eta = 1$ or $\eta = 1/2$ as the red lines in Fig. 4. For the error of 10^{-3} the measurement time t_f is 31 ns and 39 ns, respectively.

The presented results are for the coupling $g/2\pi = 30$ MHz. While the dispersion rate scales as g in the strongly nonlinear regime [see Eq. (4)], the scaling of the overall duration of the measurement process is slower than g^{-1} because of significant time needed at the initial and final stages [see Fig. 1(b)].

In this work we are not interested in how close our readout is to the quantum non-demolition (QND) measurement [29]. Notice that in the proposed implementation of the surface code [15] the measured qubits are reset, so the QNDness is not expected to be important. For the results presented in Fig. 3 the non-QNDness (probability that the initial states $|00\rangle$ and $|10\rangle$ are changed after the procedure, including the release stage) is crudely about 5%, which is mainly due to non-adiabaticity of the rear ramp of the qubit pulse. It is possible to decrease the non-QNDness significantly by using a larger rear ramp width σ_{qe} and correspondingly increasing the overall duration by several nanoseconds. However, the non-QNDness cannot be reduced below the level of few times $(g/\Delta_0)^2$, essentially because of the Purcell effect during the release stage.

Squeezing.–The JC nonlinearity causes the quadrature squeezing of the microwave field. To quantify the squeezing, we calculate the variance $\Delta x_\varphi^2 = \langle x_\varphi^2\rangle - \langle x_\varphi\rangle^2$, which can be put in the form $\Delta x_\varphi^2 = 1/4 + \langle a^\dagger a\rangle/2 - |\langle a\rangle|^2/2 + \mathrm{Re}[(\langle a^2\rangle - \langle a\rangle^2)e^{-2i\varphi}]/2$. For a coherent field $\Delta x_\varphi^2 = 1/4$, thus the state is squeezed [26] when $4\Delta x_\varphi^2 < 1$. Notice that the degree of squeezing depends on the choice of φ. However, in order to see the effect of squeezing on measurement error, we compute the squeezing along the measurement direction, $\varphi = \arg(\lambda_{eff,1} - \lambda_{eff,0})$.

Figure 5(a) shows evolution of the squeezing parameter $4\Delta x_\varphi^2$ when the initial qubit state is $|0\rangle$ (a similar result is obtained for the initial state $|1\rangle$; we again use the two-level approximation and $\eta = 1$). Notice that at first the field stays coherent, which is due to the linearity of the qubit-resonator interaction at large detuning. Later on, however, the interaction becomes nonlinear due to decreased detuning and leads to quadrature squeezing reaching the level of ∼50% for $\Delta/2\pi \lesssim 100$ MHz (see [28] for the Wigner function evolution). Figure 5(b) shows the measurement error as a func-

tion of $|\delta\lambda|$ calculated numerically (solid curves) and analytically, based on Eq. (2) (dashed curve). As expected, with the squeezing developing, the error becomes significantly smaller than the analytical prediction, for instance, up to a factor of 30 for $\Delta/2\pi = 250$ MHz. Notice also that the error shown in Fig. 5(b) saturates in spite of increasing separation $|\delta\lambda|$. This is because of the non-adiabatic error discussed above.

Conclusion.–We analyzed a fast high-fidelity readout for superconducting qubits in a cQED architecture using the controlled catch, dispersion, and release of the microwave photons. This readout uses a tunable coupler to decouple the resonator from the transmission line during the dispersion stage of the measurement, thus avoiding the Purcell effect. Our approach may also be used as a new tool to beat the standard quantum limit via self-developing field squeezing, directly measurable using the state-of-the-art parametric amplifiers.

The authors thank Farid Khalili, Konstantin Likharev, and Gerard Milburn for useful discussions. This research was funded by the Office of the Director of National Intelligence (ODNI), Intelligence Advanced Research Projects Activity (IARPA), through the Army Research Office grant W911NF-10-1-0334. All statements of fact, opinion or conclusions contained herein are those of the authors and should not be construed as representing the official views or policies of IARPA, the ODNI, or the U.S. Government. We also acknowledge support from the ARO MURI Grant W911NF-11-1-0268.

[1] K. B. Cooper, , M. Steffen, R. McDermott, R. W.Simmonds, S. Oh, D. A. Hite, D. P. Pappas, and J. M. Martinis, Phys. Rev. Lett. **93**, 180401 (2004).
[2] O. Astafiev, Yu. A. Pashkin, T. Yamamoto, Y. Nakamura, and J. S. Tsai, Phys. Rev. B **69**, 180507 (R) (2004).
[3] I. Siddiqi, R. Vijay, M. Metcalfe, E. Boaknin, L. Frunzio, R. J. Schoelkopf, and M. H. Devoret, Phys. Rev. B **73**, 054510 (2006).
[4] A. Lupascu, E. F. C. Driessen, L. Roschier, C. J. P. M. Harmans, and J. E. Mooij, Phys. Rev. Lett. **96**, 127003 (2006)
[5] F. Mallet, F. R. Ong, A. Palacios-Laloy, F. Nguyen, P. Bertet, D. Vion, and D. Esteve, Nature Phys. **5**, 791 (2009).
[6] M. D. Reed, L. DiCarlo, B. R. Johnson, L. Sun, D. I. Schuster, L. Frunzio, and R. J. Schoelkopf, Phys. Rev. Lett. **105**, 173601 (2010).
[7] A. Blais, R.-S. Huang, A. Wallraff, S. M. Girvin, and R. J. Schoelkopf, Phys. Rev. A **69**, 062320 (2004).
[8] A. Wallraff, D. I. Schuster, A. Blais, L. Frunzio, R. S. Huang, J. Majer, S. Kumar, S. M. Girvin, and R. J. Schoelkopf, Nature **431** 162 (2004).
[9] J. E. Johnson, C. Macklin, D. H. Slichter, R. Vijay, E. B. Weingarten, J. Clarke, and I. Siddiqi, Phys. Rev. Lett. **109**, 050506 (2012).
[10] D. Riste, J. G. van Leeuwen, H.-S. Ku, K. W. Lehnert, and L. DiCarlo, Phys. Rev. Lett. **109**, 050507 (2012).
[11] N. Bergeal, F. Schackert, M. Metcalfe, R. Vijay, V. E. Manucharyan, L. Frunzio, D. E. Prober, R. J. Schoelkopf, S. M. Girvin, and M. H. Devoret, Nature **465**, 64 (2010).
[12] P. Campagne-Ibarcq, E. Flurin, N. Roch, D. Darson, P. Morfin, M. Mirrahimi, M. H. Devoret, F. Mallet, and B. Huard, arXiv:1301.6095.
[13] J. Bylander, S. Gustavsson, F. Yan, F. Yoshihara, K. Harrabi, G. Fitch, D. G. Cory, Y. Nakamura, J.-S. Tsai, and W. D. Oliver, Nature Phys. **7**, 565 (2011).
[14] H. Paik, D. I. Schuster, L. S. Bishop, G. Kirchmair, G. Catelani, A. P. Sears, B. R. Johnson, M. J. Reagor, L. Frunzio, L. I. Glazman, S. M. Girvin, M. H. Devoret, and R. J. Schoelkopf, Phys. Rev. Lett. **107**, 240501 (2011).
[15] A. G. Fowler, M. Mariantoni, J. M. Martinis, and A. N. Cleland, Phys. Rev. A **86**, 032324 (2012).
[16] E. M. Purcell, Phys. Rev. **69**, 691 (1946).
[17] M. D. Reed, B. R. Johnson, A. A. Houck, L. DiCarlo, J. M. Chow, D. I. Schuster, L. Frunzio, and R. J. Schoelkopf, Appl. Phys. Lett. **96**, 203110 (2010).
[18] J. M. Gambetta, A. A. Houck, and A. Blais, Phys. Rev. Lett. **106**, 030502 (2011).
[19] R. C. Bialczak, M. Ansmann, M. Hofheinz, M. Lenander, E. Lucero, M. Neeley, A. D. O'Connell, D. Sank, H. Wang, M. Weides, J. Wenner, T. Yamamoto, A. N. Cleland, and J. M. Martinis, Phys. Rev. Lett. **106**, 060501 (2011).
[20] Y. Yin, Y. Chen, D. Sank, P. J. J. O'Malley, T. C. White, R. Barends, J. Kelly, E. Lucero, M. Mariantoni, A. Megrant, C. Neill, A. Vainsencher, J. Wenner, A. N. Korotkov, A. N. Cleland, and J. M. Martinis, arXiv:1208.2950.
[21] L. S. Bishop, E. Ginossar, and S. M. Girvin, Phys. Rev. Lett. **105**, 100505 (2010).
[22] M. Boissonneault, J. M. Gambetta, and A. Blais, Phys. Rev. Lett. **105**, 100504 (2010).
[23] Actually, for $\omega_{\rm q}(t)$ we additionally use small compensating ramps at the beginning and end of the procedure to provide the exact value ω_0 and to zero $\dot{\omega}_{\rm q}(t)$ at $t = 0$ and $t = t_{\rm f}$.
[24] A. N. Korotkov, arXiv:1111.4016.
[25] H. M. Wiseman amd G. J. Milburn, *Quantum Measurement and Control* (Cambridge Univ. Press, Cambridge, 2010), Sec. 4.7.6.
[26] M. O. Scully and M. S. Zubairy, *Quantum Optics* (Cambridge University Press, Cambridge, 1997).
[27] A. Galiautdinov, A. N. Korotkov, and J. M. Martinis, Phys. Rev. A **85**, 042321 (2012).
[28] See Supplemental Material for the Wigner function evolution.
[29] V. B. Braginsky and F. Ya. Khalili, *Quantum Measurement* (Cambridge Univ. Press, 1992).